

Using Fractal Scaling and Two-Dimensional Particle Size Spectra to Calculate Coagulation Rates for Heterogeneous Systems

George A. Jackson¹

Department of Oceanography, Texas A&M University, College Station, TX 77843

Received December 13, 1996; accepted January 23, 1998

Fractal scaling is usually presented as a relationship between aggregate mass and length. Such scaling can also be expressed as a relationship between the lengths of two particles that collide and the length of the resulting aggregate. Emphasizing fractal scaling as a geometric property allows the extension of fractal description to aggregates composed of more than one type of source particle. In particular, it allows the development of more complete models of the role of coagulation in marine ecosystems. The classical aggregation equations can be modified to accommodate a two-dimensional particle size spectrum. This two-dimensional set of equations can be solved using a modification of the sectional approach. Because moving to two-dimensions vastly increases the number of possible interactions and makes solution more computationally costly, simplifications that decrease the allowable interactions considerably speed up the calculations for relatively little loss of accuracy. © 1998 Academic Press

Key Words: fractal; heterodisperse distribution; coagulation; aggregation; simulations; particle size spectra; sectional approach.

INTRODUCTION

The use of fractal scaling has been an important advance in describing aggregate structure. By starting with monodisperse particle distributions, moving particles using simple rules, and combining particles after they collide, computer simulations have shown that there are simple relationships between the length and the number of monomers (equivalent to mass) in simulated aggregates (*e.g.*, 1, 2). Among the implications of fractal scaling is that aggregate length increases more rapidly than the cube root of aggregate mass.

The coagulation processes of differential sedimentation and shear coagulation are physically more complicated than the numerical simulations of fractal formation, which have emphasized diffusion, but experimental observations have shown that aggregates formed by them have similar fractal scaling between mass and length (3, 4). However, natural systems can have multiple sources of particles capable of coagulating with each other. A particle with a given mass

need not have a unique length associated with it. Aggregates formed in such systems should have the increasing porosity as a function of size characteristic of fractal scaling. Unfortunately, the scaling rules derived from monodisperse systems are not directly applicable to these systems.

In the development of models describing coagulation and the dynamics of particle size spectra, particle mass and diameter are the two most important properties. Mass is usually the quantity of interest and is the property conserved in particle interactions; length determines the interactions of a particle with its environment, including neighboring particles. Fractal scaling provides a means of calculating a particle's length from its mass for the initially monodisperse system but not for the heterodisperse system.

Models of aggregation in marine systems have emphasized the aggregation of marine algal blooms, systems which should approximate monodisperse conditions (*e.g.*, 5–7). The multiple particle sources evident in many marine aggregates (8) suggest that theories that can describe the interactions of multiple particle sources also need to be developed. Heterodisperse sources may be needed to describe even the simple case of algal bloom aggregation. Chemical analyses of marine snow have shown the presence of transparent organic matter (TEP) which had been undetectable before the development of special staining procedures (9). Such material may result from the aggregation of colloidal organic carbon particles (10) or from mucus leakage by diatoms (9, 11). In either case, TEP could alter algal coagulation rates by increasing particle concentrations or by changing algal stickiness (11, 12). In addition, the presence of gas bubbles within marine snow can affect coagulation by inhibiting particle removal by settling from the mixed layer (13). These bubbles should also affect aggregate sinking rates, thereby changing rates of aggregate collision through differential sedimentation.

The importance of multiple particle sources in the aquatic environment implies that coagulation models describing their dynamics must incorporate them as part of the fractal scaling relationships.

In this paper, I describe a method for extending fractal scaling considerations to describe the lengths of aggregates

¹ To whom correspondence should be addressed.

TABLE 1
Definition of Sectional Coagulation Coefficients^a

Symbol	Range	Value
${}^1\bar{\beta}_{ijl}$	$i < l - 1, j < l - 1, 2 \leq l \leq s$	0
	$i \leq l - 1, j = l - 1, 2 \leq l \leq s$	$\frac{1}{m_{i-1}m_{l-2}} \int_{m_{i-1}}^{m_i} \int_{m_{l-1}-\bar{m}_1}^{m_{l-1}} \frac{(\bar{m}_1 + \bar{m}_2)\beta(\bar{m}_1, \bar{m}_2)}{\bar{m}_1\bar{m}_2} d\bar{m}_2 d\bar{m}_1$
	$i = l - 1, j = l - 1, 2 \leq l \leq s$	$\frac{1}{2m_{l-2}^2} \int_{m_{i-2}}^{m_{i-1}} \int_{m_{i-2}}^{m_{i-1}} \frac{(\bar{m}_1 + \bar{m}_2)\beta(\bar{m}_1, \bar{m}_2)}{\bar{m}_1\bar{m}_2} d\bar{m}_2 d\bar{m}_1$
${}^2\bar{\beta}_{ijl}$	$i < l, j = l, 2 \leq l \leq s$	$\frac{1}{m_{i-1}m_{l-1}} \int_{m_{i-1}}^{m_i} \int_{m_{i-1}-\bar{m}_1}^{m_i} \frac{\beta(\bar{m}_1, \bar{m}_2)}{\bar{m}_1} d\bar{m}_2 d\bar{m}_1$
		$- \frac{1}{m_{i-1}m_{l-1}} \int_{m_{i-1}}^{m_i} \int_{m_{i-1}}^{m_i-\bar{m}_1} \frac{\beta(\bar{m}_1, \bar{m}_2)}{\bar{m}_2} d\bar{m}_2 d\bar{m}_1$
${}^3\bar{\beta}_{ijl}$	$i = j = l, 1 \leq l \leq s$	$\frac{1}{2m_{l-1}^2} \int_{m_{i-1}}^{m_i} \int_{m_{i-1}}^{m_i} \frac{(\bar{m}_1 + \bar{m}_2)\beta(\bar{m}_1, \bar{m}_2)}{\bar{m}_1\bar{m}_2} d\bar{m}_2 d\bar{m}_1$
${}^4\bar{\beta}_{ijl}$	$l < i, j = l, 1 \leq l \leq s$	$\frac{1}{m_{i-1}m_{l-1}} \int_{m_{i-1}}^{m_i} \int_{m_{i-1}}^{m_i} \frac{\beta(\bar{m}_1, \bar{m}_2)}{\bar{m}_1} d\bar{m}_2 d\bar{m}_1$

^a These have been derived from those of Gelbard *et al.* (16) for the case of mass conservation.

formed from source particles of different masses and lengths. I then extend a numerical approach for calculating the temporal evolution of particle size spectra for one dimension to a two-dimensional approach that describes particle in terms of both their masses and a length-related parameter. Because the computational cost of describing particle interactions for the two-dimensional particle size spectrum is very high, I also develop a simplified description of the particle dynamics that can save considerable computational resources. I end with numerical calculations comparing the results from the new approaches.

THEORY

A Conservative Fractal Quantity During Collisions

For an aggregate consisting of i identical spherical particles, each of mass m_1 , the aggregate length L_i (usually stipulated as the radius of gyration) is given by

$$m_i = im_1 = bL_i^D \quad [1]$$

where D is the cluster fractal dimension and b is a constant (e.g., 2, 14). For three-dimensional particles that conserve total particle volume when they aggregate, $D = 3$. An example of this occurs when water droplets collide and form a new droplet. D is usually less than 3 when the particles are solids in a fluid environment.

The value of D determined in a simulation depends on details of particle interactions. When only monomers diffuse to a single expanding particle, in what is known as diffusion

limited aggregation (DLA), D may be 2.5; when initially monodisperse particles are allowed to collide with each other to form a distribution of ever-increasing particle sizes, in what is known as cluster-cluster aggregation (CCA), D may be 1.75 (2).

For an aggregate formed by the collision of aggregates with i and j monomers in CCA, the length of the new particle is determined from mass conservation and Eq. [1] as

$$L_{i+j}^D = L_i^D + L_j^D. \quad [2]$$

The elimination of the constant b associated with the monomer size suggests that Eq. [2] is an alternate statement of fractal scaling of aggregates that is purely geometric. That is, the length of an aggregate formed in CCA is a function only of the lengths of the two particles colliding to form it, not of their masses.

Equation [2] further suggests that

$$\lambda \equiv L^D \quad [3]$$

is a fundamental, conserved quantity of the aggregation interaction. Hence,

$$\lambda_{ij} = \lambda_i + \lambda_j. \quad [4]$$

For the case of aggregates formed from monodisperse particles, this is equivalent to mass conservation. Where it becomes something new is with aggregates formed from initially heterodisperse particles, where λ provides a property separate from mass that is conserved as particles coagulate.

TABLE 2
Particle Number and Mass Spectral Distributions for Different
Functions $f(m)$ and $g(\lambda)^a$

$f(m)$	$g(\lambda)$	$n(m, \lambda, t)$	$\bar{q}_l(t)$
m	λ	$\frac{Q_k(t)}{mm_{l-1}\lambda_{k-1}}$	$\frac{Q_k(t)}{m_{l-1}\lambda_{k-1}}$
m	$\ln \lambda$	$\frac{Q_k(t)}{m\lambda m_{l-1} \ln(2)}$	$\frac{Q_k(t)}{\lambda m_{l-1} \ln(2)}$

^a The formula assume that $m_l = 2m_{l-1}$ and $\lambda_k = 2\lambda_{k-1}$.

Consider how particle 1, an aggregate composed of 10^6 monomers, each with m_0 and $L_0 = 1$, has a different length ($L_1 = 1000$ and $\lambda_1 = 10^6$ for $D = 2$) but the same mass ($m_1 = m_2 = 10^6$) as a particle 2, a monomer with $m_2 = 10^6$ and $L_2 = 100$ ($\lambda_2 = 10^4$). Despite having the same masses, the particles have different lengths. Aggregates formed from the collision of two particle 1s (1_{11}), one particle 1 and one particle 2 (1_{12}), and two particle 2s (2_{22}) have the same mass ($m_{11} = m_{12} = m_{22} = 2 \times 10^6$) but have different values of λ ($\lambda_{11} = 2 \times 10^6$, $\lambda_{12} = 1.01 \times 10^6$, and $\lambda_{22} = 2 \times 10^4$) and length ($L_{11} = 1.4 \times 10^3$, $L_{12} = 1.005 \times 10^3$, and $L_{22} = 1.4 \times 10^2$). Conservation of λ allows us to calculate the lengths of the different aggregates independently of their masses.

The standard description of particle distribution is the particle size spectrum $n(m)$, where $n(m)dm$ is the number of particles between m and $m + dm$ (15). Changes in $n(m)$ are given by

$$\begin{aligned} \frac{dn(m)}{dt} = & 0.5 \int_0^m \beta(\bar{m}, m - \bar{m}) n(\bar{m}) n(m - \bar{m}) d\bar{m} \\ & - \int_0^\infty \beta(\bar{m}, m) n(\bar{m}) n(m) d\bar{m} \end{aligned} \quad [5]$$

The development of a conserved length measure allows the use of two-dimensional particle size spectrum $n(m, \lambda)$, where the number concentration of particles in the range of m to $m + dm$, λ to $\lambda + d\lambda$ is $n(m, \lambda) dm d\lambda$. The extension of Eq. [3] to include two-dimensional particle spectra is given by

$$\begin{aligned} \frac{dn(m, \lambda)}{dt} = & 0.5 \int_0^m \int_0^\lambda \beta(\bar{m}, m - \bar{m}, \bar{\lambda}, \lambda - \bar{\lambda}) n(\bar{m}, \bar{\lambda}) \\ & \times n(m - \bar{m}, \lambda - \bar{\lambda}) d\bar{m} d\bar{\lambda} \\ & - \int_0^\infty \int_0^\infty \beta(\bar{m}, m, \bar{\lambda}, \lambda) n(\bar{m}, \bar{\lambda}) \\ & \times n(m, \lambda) d\bar{m} d\bar{\lambda} \end{aligned} \quad [6]$$

The Sectional Approach to Solving the One-Dimensional Particle Coagulation Problem

Gelbard *et al.* (16) developed a technique for solving the one-dimensional coagulation equation [5] numerically in an efficient manner by transforming it to a problem of solving for the distribution of particle mass within finite particle size intervals, known as sections. The approach outlined here is an application of their more generalized development for the one-dimensional equation.

Start by dividing the particle mass range m into contiguous intervals, where the upper and lower bounds of the l th interval are m_l and m_{l-1} . The particle mass distribution $q(m, t)$ is given by

$$q(m, t) = mn(m, t) \quad [7]$$

where $n(m, t)$ is again the particle size spectrum. The total mass concentration in the l th section $Q_l(t)$ is given by

$$Q_l(t) = \int_{m_{l-1}}^{m_l} q(m, t) dm. \quad [8]$$

Assume that q can be separated into functions of t and m :

$$q(m, t) = \bar{q}_l(t) f'(m) \quad [9]$$

where $f'(m) = df/dm$ and $m_{l-1} < m < m_l$. Substituting Eq. [9] into Eq. [8] and integrating yields

$$\begin{aligned} Q_l(t) = & \bar{q}_l(t) [f(m_l) - f(m_{l-1})] \\ & \text{for } m_{l-1} < m < m_l \end{aligned} \quad [10]$$

and

$$\begin{aligned} n(m, t) = & \frac{Q_l(t) f'(m)}{m [f(m_l) - f(m_{l-1})]} \\ & \text{for } m_{l-1} < m < m_l. \end{aligned} \quad [11]$$

There are three ways collisions between particles of mass \bar{m}_1 and \bar{m}_2 move mass in or out of the l th section: first, collisions between two particles with masses below the section lower limit ($\bar{m}_1 < m_{l-1}$ and $\bar{m}_2 < m_{l-1}$) that produce a particle with a mass in the l th section ($m_{l-1} < (\bar{m}_1 + \bar{m}_2) < m_l$) and which add both masses to the l th section; second, collisions between one particle with mass below the lower section limit ($\bar{m}_1 < m_{l-1}$) and one in the section ($m_{l-1} < \bar{m}_2 < m_l$) which add the mass of the smaller particle to the l th section ($m_{l-1} < \bar{m}_1 + \bar{m}_2 < m_l$); and third, collisions between particles of any mass \bar{m}_1 and a particle in the section ($m_{l-1} < \bar{m}_2 < m_l$) that removes mass by forming a particle whose mass is greater than the sectional bound ($m_l < \bar{m}_1 + \bar{m}_2$). The third collision type can be further subdivided into the cases where $\bar{m}_1 < m_{l-1}$ and only some collisions remove

TABLE 3
Interaction Coefficients for Two-Dimensional Spectra^a

$$\begin{aligned}
 {}^1\hat{\beta}_{k_1,k_2,k_3,l_1,l_2,l_3} &= \eta_{l_1}\eta_{l_2}\zeta_{k_1}\zeta_{k_2} \int_{\lambda_{k_2-l_1}}^{\lambda_{k_2}} \int_{\lambda_{k_1-l_1}}^{\lambda_{k_1}} \int_{m_{l_2-1}}^{m_{l_2}} \int_{m_{l_1-1}}^{m_{l_1}} \theta(\lambda_{k_3-l_1} < \bar{\lambda}_1 + \bar{\lambda}_2 < \lambda_{k_3})\theta(m_{l_3-1} < \bar{m}_1 + \bar{m}_2 < m_{l_3})(\bar{m}_1 + \bar{m}_2)g'(\bar{\lambda}_1)g'(\bar{\lambda}_2)f'(\bar{m}_1)f'(\bar{m}_2)\beta(\bar{m}_1, \bar{m}_2, \bar{\lambda}_1, \bar{\lambda}_2) \\
 &\quad d\bar{m}_1 d\bar{m}_2 d\bar{\lambda}_1 d\bar{\lambda}_2 \quad \text{for } (l_1 \neq l_3, k_1 \neq k_3) \\
 &= \eta_{l_1}\eta_{l_2}\zeta_{k_1}\zeta_{k_2} \int_{\lambda_{k_2-l_1}}^{\lambda_{k_2}} \int_{\lambda_{k_1-l_1}}^{\lambda_{k_1}} \int_{m_{l_2-1}}^{m_{l_2}} \int_{m_{l_1-1}}^{m_{l_1}} \theta(\bar{\lambda}_1 + \bar{\lambda}_2 < \lambda_{k_3})\theta(\bar{m}_1 + \bar{m}_2 < m_{l_3})\bar{m}_2 g'(\bar{\lambda}_1)g'(\bar{\lambda}_2)f'(\bar{m}_1)f'(\bar{m}_2)\beta(\bar{m}_1, \bar{m}_2, \bar{\lambda}_1, \bar{\lambda}_2) d\bar{m}_1 d\bar{m}_2 d\bar{\lambda}_1 d\bar{\lambda}_2 \\
 &\quad \text{for } (l_1 < l_3) \text{ and } (k_1 = k_3) \\
 {}^2\hat{\beta}_{k_1,k_2,l_1,l_2} &= \eta_{l_1}\eta_{l_2}\zeta_{k_1}\zeta_{k_2} \int_{\lambda_{k_2-l_1}}^{\lambda_{k_2}} \int_{\lambda_{k_1-l_1}}^{\lambda_{k_1}} \int_{m_{l_2-1}}^{m_{l_2}} \int_{m_{l_1-1}}^{m_{l_1}} \theta([m_{k_1} < \bar{m}_1 + \bar{m}_2] \text{ or } [\lambda_{k_1} < \bar{\lambda}_1 + \bar{\lambda}_2])\bar{m}_1 g'(\bar{\lambda}_1)g'(\bar{\lambda}_2)f'(\bar{m}_1)f'(\bar{m}_2)\beta(\bar{m}_1, \bar{m}_2, \bar{\lambda}_1, \bar{\lambda}_2) d\bar{m}_1 d\bar{m}_2 d\bar{\lambda}_1 d\bar{\lambda}_2 \\
 &\quad \text{for } (l_1 \neq l_2) \text{ and } (k_1 \neq k_2) \\
 &= 0.5\eta_{l_1}^2\zeta_{k_1}^2 \int_{\lambda_{k_2-l_1}}^{\lambda_{k_2}} \int_{\lambda_{k_1-l_1}}^{\lambda_{k_1}} \int_{m_{l_2-1}}^{m_{l_2}} \int_{m_{l_1-1}}^{m_{l_1}} (\bar{m}_1 + \bar{m}_2)g'(\bar{\lambda}_1)g'(\bar{\lambda}_2)f'(\bar{m}_1)f'(\bar{m}_2)\beta(\bar{m}_1, \bar{m}_2, \bar{\lambda}_1, \bar{\lambda}_2) d\bar{m}_1 d\bar{m}_2 d\bar{\lambda}_1 d\bar{\lambda}_2 \\
 &\quad \text{for } (l_1 = l_2) \text{ and } (k_1 = k_2)
 \end{aligned}$$

^a The interactions coefficient ${}^1\hat{\beta}_{k_1,k_2,k_3,l_1,l_2,l_3}$ is given for those interactions between particles in sections (k_1, l_1) and (k_2, l_2) which add material to compartment (k_3, l_3) and ${}^2\hat{\beta}_{k_1,k_2,k_3,l_1,l_2,l_3}$ for those interactions which remove material from (k_3, l_3) . Calculations made assume that $m_l = 2m_{l-1}$ and $\lambda_k = 2\lambda_{k-1}$. $\eta_l = [f(m_l) - f(m_{l-1})]^{-1}$, $\zeta_k = [g(m_k) - g(m_{k-1})]^{-1}$.

mass from a section, where both particles are in the l th section, all collisions remove mass and the mass of both particles is removed, and where $m_l < \bar{m}_1$ and all collisions remove mass from the section. These considerations lead to an equation describing changes in Q_l as

$$\begin{aligned}
 \frac{dQ_l}{dt} &= + \frac{1}{2} \int_{m_0}^{m_{l-1}} \int_{m_0}^{m_{l-1}} \theta\{m_{l-1} < \bar{m}_1 + \bar{m}_2 < m_l\} \\
 &\quad \times (\bar{m}_1 + \bar{m}_2)\beta(\bar{m}_1, \bar{m}_2)n(\bar{m}_1, t)n(\bar{m}_2, t)d\bar{m}_2 d\bar{m}_1 \\
 &\quad + \int_{m_0}^{m_{l-1}} \int_{m_{l-1}}^{m_l} \theta\{m_{l-1} < \bar{m}_1 + \bar{m}_2 < m_l\} \\
 &\quad \times \bar{m}_1\beta(\bar{m}_1, \bar{m}_2)n(\bar{m}_1, t)n(\bar{m}_2, t)d\bar{m}_2 d\bar{m}_1 \\
 &\quad - \int_{m_0}^{m_{l-1}} \int_{m_{l-1}}^{m_l} \theta\{m_l < \bar{m}_1 + \bar{m}_2\} \bar{m}_2\beta(\bar{m}_1, \bar{m}_2) \\
 &\quad \times n(\bar{m}_1, t)n(\bar{m}_2, t)d\bar{m}_2 d\bar{m}_1 \\
 &\quad - \frac{1}{2} \int_{m_{l-1}}^{m_l} \int_{m_{l-1}}^{m_l} \theta\{m_l < \bar{m}_1 + \bar{m}_2\} (\bar{m}_1 + \bar{m}_2) \\
 &\quad \times \beta(\bar{m}_1, \bar{m}_2)n(\bar{m}_1, t)n(\bar{m}_2, t)d\bar{m}_2 d\bar{m}_1 \\
 &\quad - \int_{m_l}^{m_s} \int_{m_{l-1}}^{m_l} \bar{m}_2\beta(\bar{m}_1, \bar{m}_2)n(\bar{m}_1, t)n(\bar{m}_2, t)d\bar{m}_2 d\bar{m}_1
 \end{aligned}$$

[12]

where $\theta = 1$ when the condition inside the braces is met and $\theta = 0$ otherwise, s is the number of sections spanning the range of interest, and m_0 is the smallest particle considered.

Because n is defined in a piecewise manner, the integrals in Eq. [12] can be broken into sums of integrals, each integral spanning the range of one section. Furthermore, because the m -varying part of $n(m, t)$ is independent of time (Eq.

[11]), the integrals can be solved separately from the differential equations describing $Q_l(t)$. Solving the resulting set of differential equations still constitutes a substantial technical problem.

If the upper limit of a section is equal to or greater twice the lower limit, $m_l \geq 2m_{l-1}$, one of the particles in the collision must come from either the $l-1$ or the l section for the summed mass to be within the l th section. Setting $m_l = 2m_{l-1}$, using Eq. [11] on Eq. [12] and consolidating terms for interactions between the same sections results in

$$\begin{aligned}
 \frac{dQ_l}{dt} &= Q_{l-1} \sum_{i=1}^{l-1} {}^1\bar{\beta}_{i,l-1,l}Q_i - Q_l \sum_{i=1}^{l-1} 2{}^2\bar{\beta}_{i,l,l}Q_i \\
 &\quad - {}^3\bar{\beta}_{l,l,l}Q_l^2 - Q_l \sum_{i=l+1}^s 4{}^4\bar{\beta}_{i,l,l}Q_i \quad [13]
 \end{aligned}$$

where s is the total number of sections, ${}^1\bar{\beta}_{i,j,l}$, ${}^2\bar{\beta}_{i,l,l}$, ${}^3\bar{\beta}_{l,l,l}$, ${}^4\bar{\beta}_{i,l,l}$ are the sectional coagulation coefficients defined in (16). Their values for the case of $f(m) = m$ are shown in Table 1. The number of terms to be calculated evaluating dQ_l/dt is $\sim s$. The total number of terms that needs to be calculated when evaluating all s derivatives is $\sim s^2$.

The transformation resulting from Eq. [11] changes the problem of describing system dynamics from evaluating an integro-differential equation into solving a finite number of coupled ordinary differential equations. The latter problem can be readily solved with numerical differential equation solvers. While there are numerous integrals to be evaluated for the $\bar{\beta}$ coefficients, the evaluations need to be done only once as part of an initialization procedure. The result of the sectional transformation is a quite efficient numerical method for determining the evolution of a particle size spectrum.

A Sectional Approach to the Two-Dimensional Particle Spectrum

The equation for the development of the two-dimensional particle size spectrum (Eq. [6]) can be solved numerically by extending the sectional approach of Gelbard *et al.* (16) to two dimensions. For a particle size spectrum $n(m, \lambda, t)$, the particle mass distribution $q(m, \lambda, t)$ is given by

$$\begin{aligned} q(m, \lambda, t) &= mn(m, \lambda, t) \\ &= \bar{q}_{kl}(t) f'(m) g'(\lambda) \end{aligned} \quad [14]$$

where Eq. [14] assumes that $q(m, \lambda, t)$ can be separated into functions of t , m , and λ , ($m_{l-1} < m < m_l$, $\lambda_{k-1} < \lambda < \lambda_k$), and where $f'(m) = df(m)/dm$ and $g'(\lambda) = dg(\lambda)/d\lambda$. Examples are shown in Table 2.

The total mass in the interval is

$$\begin{aligned} Q_{kl}(t) &= \int_{\lambda_{k-1}}^{\lambda_k} \int_{m_{l-1}}^{m_l} mn(m, \lambda, t) dmd\lambda \\ &= \int_{\lambda_{k-1}}^{\lambda_k} \int_{m_{l-1}}^{m_l} \bar{q}_{kl}(t) f'(m) g'(\lambda) dmd\lambda \\ &= \bar{q}_{kl}(t) [f(m_l) - f(m_{l-1})] [g(\lambda_k) - g(\lambda_{k-1})]. \end{aligned} \quad [15]$$

Hence, for $m_{l-1} < m < m_l$, $\lambda_{k-1} < \lambda < \lambda_k$,

$$\bar{q}_{kl}(t) = \frac{Q_{kl}}{[f(m_l) - f(m_{l-1})][g(\lambda_k) - g(\lambda_{k-1})]} \quad [16]$$

$$\begin{aligned} n(m, \lambda, t) &= Q_{kl}(t) \frac{f'(m)}{m[f(m_l) - f(m_{l-1})]} \\ &\quad \times \frac{g'(\lambda)}{[g(\lambda_k) - g(\lambda_{k-1})]} \end{aligned} \quad [17]$$

$$\begin{aligned} \frac{dQ_{k,l}}{dt} &= 0.5 \sum_{k_1=1}^k \sum_{k_2=1}^k \sum_{l_1=1}^l \sum_{l_2=1}^l {}^1\hat{\beta}_{k_1,k_2,k,l_1,l_2,l} Q_{k_1,l_1} Q_{k_2,l_2} \\ &\quad - \sum_{k_2=1}^{k_{max}} \sum_{l_2=1}^{l_{max}} {}^2\hat{\beta}_{k,k_2,l,l_2} Q_{k,l} Q_{k_2,l_2} \end{aligned} \quad [18]$$

where the definitions for ${}^1\hat{\beta}_{k_1,k_2,k,l_1,l_2,l}$, and ${}^2\hat{\beta}_{k,k_2,l,l_2}$ are given in Table 3. Notice that these $\hat{\beta}$ are different than those of Eq. [13] because of a consolidation of terms. The two-dimensional approach involves significantly more calculations than the comparable one-dimensional system, $\sim s^4$ for each equation and $\sim s^6$ for the system, where $s = k_{max} = l_{max}$ and there are s^2 sections.

As in the one-dimensional case, the assumption that $m_l \geq 2m_{l-1}$ and $\lambda_k \geq 2\lambda_{k-1}$ reduces the number of interactions which must be considered when calculating $dQ_{k,l}/dt$ because conservation of m and λ require that at least one of the two particles in a collision that forms a particle in (k, l) is in

the $l-1$ or l and is in the k or $k-1$ sections. As a result, the number of interactions which affect $Q_{kl}(t)$ is $\sim s^2$. To describe all the interactions, there are only $\sim s^4$ interactions. The problem is further simplified by assuming that the upper section bounds are twice the lower bounds ($m_l = 2m_{l-1}$, $\lambda_k = 2\lambda_{k-1}$), although this assumption does not significantly change the outcome. The resulting equation describing the changes in sectional concentration is

$$\begin{aligned} \frac{dQ_{k,l}}{dt} &= \sum_{k_2=1}^{k-1} \sum_{l_2=1}^{l-1} (1 - 0.5\delta_{k-1,k_2} \delta_{l-1,l_2}) \\ &\quad \times {}^1\hat{\beta}_{k-1,k_2,k,l-1,l_2,l} Q_{k-1,l-1} Q_{k_2,l_2} \\ &\quad + \sum_{k_2=1}^{k-1} \sum_{l_2=1}^{l-1} (1 - 0.5\delta_{k-1,k_2} \delta_{l-1,l_2}) \\ &\quad \times {}^1\hat{\beta}_{k_2,k-1,k,l-1,l_2,l} Q_{k_2,l-1} Q_{k-1,l_2} \\ &\quad + \sum_{k_2=1}^{k-1} \sum_{l_2=1}^{l-1} {}^1\hat{\beta}_{k,k_2,k,l-1,l_2,l} Q_{k,l-1} Q_{k_2,l_2} \\ &\quad + \sum_{k_2=1}^{k-1} \sum_{l_2=1}^{l-1} {}^1\hat{\beta}_{k_2,k,k,l-1,l_2,l} Q_{k_2,l-1} Q_{k,l_2} \\ &\quad + \sum_{k_2=1}^{k-1} \sum_{l_2=1}^{l-1} {}^1\hat{\beta}_{k-1,k_2,k,l,l_2,l} Q_{k-1,l} Q_{k_2,l_2} \\ &\quad + \sum_{k_2=1}^{k-1} \sum_{l_2=1}^{l-1} {}^1\hat{\beta}_{k_2,k-1,k,l,l_2,l} Q_{k_2,l} Q_{k-1,l_2} \\ &\quad + \sum_{k_2=1}^{k-1} \sum_{l_2=1}^{l-1} {}^1\hat{\beta}_{k,k_2,k,l,l_2,l} Q_{k,l} Q_{k_2,l_2} \\ &\quad + \sum_{k_2=1}^{k-1} \sum_{l_2=1}^{l-1} {}^1\hat{\beta}_{k_2,k,k,l,l_2,l} Q_{k_2,l} Q_{k,l_2} \\ &\quad - Q_{k,l} \sum_{k_2=1}^{k_{max}} \sum_{l_2=1}^{l_{max}} {}^2\hat{\beta}_{k,k_2,l,l_2} Q_{k_2,l_2} \end{aligned} \quad [19]$$

where the factors with δ_{k-1,k_2} , δ_{l-1,l_2} (the Kronecker delta) are used to avoid double counting interactions. The definitions for the ${}^1\hat{\beta}$, ${}^2\hat{\beta}$ are in Table 3 (notation in Table 4).

Thus, the sectional approach for the calculation of one-dimensional particle size spectra can be extended to provide a transformation of the two-dimensional coagulation equation to a series of coupled ordinary differential equations. While this does make the computational problem more tractable, it does greatly increase the computational burden over that of the one-dimensional sectional approach.

Decreasing the Computational Cost of the 2-D Sectional Approach

Although the two-dimensional spectrum and sectional approaches allow significantly more particle classes than do

TABLE 4
Notation

Symbol	Meaning
d	Particle diameter
D	Fractal dimension
\hat{D}	Diffusion coefficient
$I_{k,l}$	Particle source
k	Boltzmann constant
L	Aggregate length
m	Mass of a particle
m_1	Mass of a unit particle
\hat{m}_i	Particle mass of upper bound for section k
n	Particle number spectrum
N	Number concentration of particles larger than a given size
q	Particle mass spectrum
\hat{q}_l, \hat{q}_{kl}	Time-varying part of sectional spectrum
Q_i	Total mass concentration of particulate material in section i
r	Particle radius
\hat{r}	Effective interaction particle radius
s	Number of sectional divisions in m or λ
r_h	Hydraulic radius (effective radius for drag)
t	Time
T	Temperature
v	Particle volume
w	Particle fall velocity
Z	Mixed layer depth
β_{ij}	Coagulation kernel
β_{Br}	Brownian motion coagulation kernel
β_{ds}	Differential sedimentation coagulation kernel
β_{sh}	Shear coagulation kernel for particles with masses m_i, m_j
${}^1\beta_{i,l}, {}^2\beta_{i,l}$	Sectional interaction coefficients for 1D spectra
${}^3\beta_{i,l}, {}^4\beta_{i,l}$	Sectional interaction coefficients for 2D spectra
${}^1\beta_{k_1,k_2,k_3,l_1,l_2,l_3}$	Sectional interaction coefficients for 2D spectra
${}^2\beta_{k_1,k_2,l_1,l_2}$	Sectional interaction coefficients for 2D spectra
η	Dynamic viscosity
γ	Shear rate
λ	Conserved fractal size
μ	Particle specific growth rate
ν	Kinematic viscosity

the analogous one-dimensional descriptions, not all of the sections are equally important. For example, the aggregates formed from an initially monodisperse system should all have $\lambda \propto m$ (Eq. [1]). In a plot of m versus λ , all the particles would lie along a straight line. For the two-dimensional sectional approach in which $m_l = 2m_{l-1}$ and $\lambda_k = 2\lambda_{k-1}$, the m - λ line manifests itself as a diagonal across a two-dimensional grid (Fig. 1). Aggregates formed from two different particle sources coagulating independently of each other should form two diagonals on a two-dimensional sectional grid. Aggregates formed from the interaction of these two particle types have m and λ that lie on diagonals between the two diagonals (Fig. 1).

The actual solution of two-dimensional sectional equations generates particles in off-diagonal sections. Representing particles as being initially ‘‘monodisperse’’ in the two-

dimensional sectional approach involves assigning their mass to a single section which has particles with a range of values for both m and λ . Such a spread decreases the monodispersity of the initial distribution and results in particles that do not strictly conform to $m \sim \lambda$ relationship. Furthermore, numerical dispersion causes the material to spread into nondiagonal sections during coagulation.

For these reasons, it is an approximation to constrain aggregates to exist between the diagonals formed by multiple particle sources for a two-dimensional sectional calculation in what is denoted here as the *diagonal constraint* (DC). A calculation using all sections in a two-dimensional sectional grid is denoted as a *full grid* calculation (FG). The DC approximation can significantly decrease the number of sections for which interactions must be calculated. As noted earlier, the full grid procedure requires $\sim s^4$ terms to evaluate all derivatives in Eq. [19]. Decreasing the effective number of sections by half decreases the number of required calculations by three fourths.

An Example of the Use of the 2-D Sectional Approach

Marine ecosystems powered by micro-algae provide situations where multiple particle sources are important (e.g., 17,

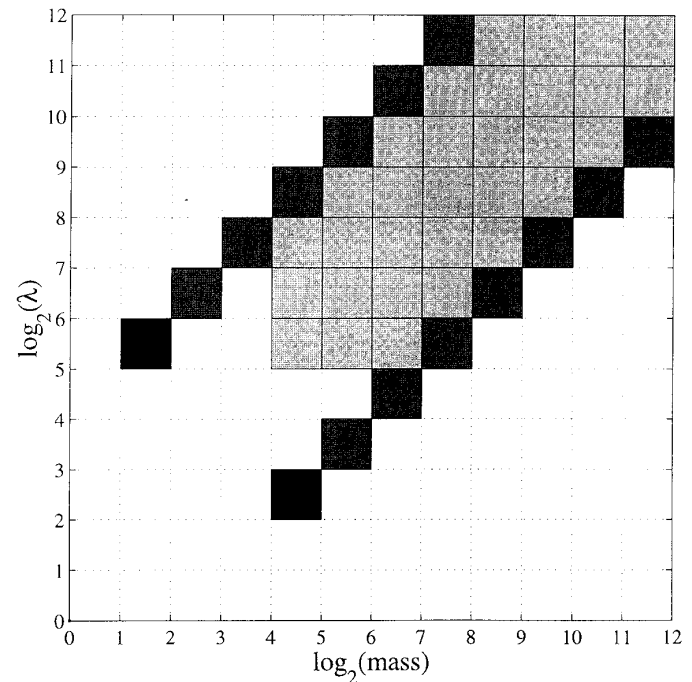


FIG. 1. Schematic of allowable interactions. The darkest squares at ($k = 5, l = 3$) and ($k = 2, l = 6$) represent sections in which source particles are formed. The diagonals with intermediate shading represent the sections in which new particles would be formed by coagulation if there were no interaction between the two sources. Lighter gray region represents the sections where particle mass is formed by the interactions between the sources and their diagonals. Implicit in this diagram is that $m_l = 2m_{l-1}$ and $\lambda_k = 2\lambda_{k-1}$.

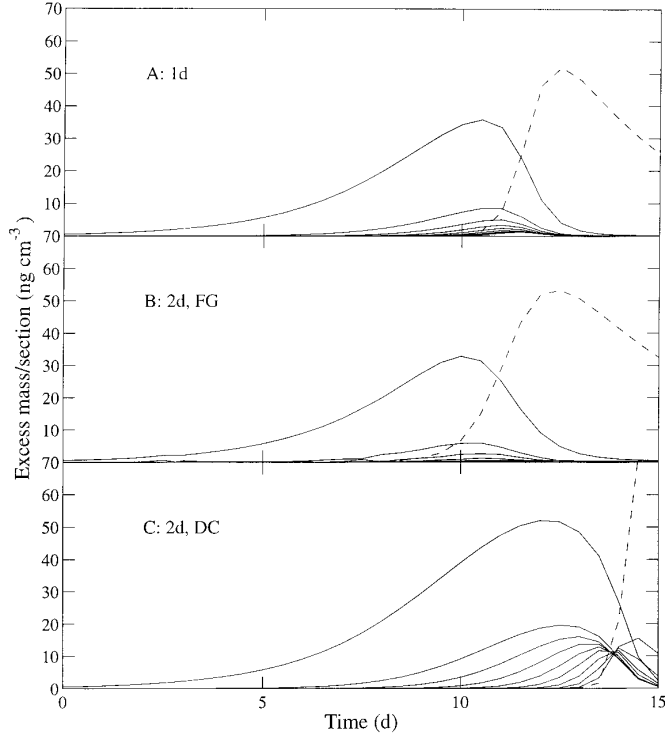


FIG. 2. Excess mass distribution in time for different methods of calculating the spectrum for a single particle source in the section with smallest m and λ ($I_{1,1} = \mu Q_{1,1}$, $I_{k,l} = 0$ for $(k, l) \neq (1, 1)$). A: one-dimensional particle spectrum approach with 10 sections (Eq. [13]); B: two-dimensional approach with full grid; C: two-dimensional approach with diagonal constraint. Lines in B and C represent the sum of concentrations for all λ sections with a given mass sectional parameter l calculated using a 10 by 10 section two-dimensional spectrum [$\bar{q}_{kl}(t) = Q_{kl}(t)/(\lambda m_{l-1} \ln(2))$]. Collisions that subtract mass from one section are allowed only if they add it to a section within the acceptable range. Dashed lines indicate matter that accumulates in the largest sections. For $t < 11$ d, sections with smaller particles have higher mass concentrations. $\mu = 0.5 \text{ d}^{-1}$, $\gamma = 0.5 \text{ s}^{-1}$, $Z = 100 \text{ m}$, $a_0 = 5 \text{ }\mu\text{m}$, $m_0 = 0.15 \text{ ng}$.

18). Algal growth can provide an exponentially increasing particle source. Additional particles can be formed from organic material that they release, animal fecal pellets, and all the other particulate residue of living organisms. Release of colloidal organic material by phytoplankton can provide for simultaneous production of two different particle types.

Classic coagulation models emphasize three mechanisms for particle-particle contact—Brownian diffusion, laminar and turbulent shear, and differential sedimentation—which are assumed to act independently. Using the subscripts Br , sh , and ds to denote the different mechanisms, the total interaction is given by (19)

$$\beta_{ij} = \beta_{Br,ij} + \beta_{sh,ij} + \beta_{ds,ij}. \quad [20]$$

The rectilinear formulations, in which the particles are assumed to move independently until they collide, are used here (19):

$$\beta_{sh,ij} = 1.3\gamma(\hat{r}_i + \hat{r}_j)^3 \quad [21]$$

$$\beta_{Br,ij} = 4\pi(\hat{D}_i + \hat{D}_j)(\hat{r}_i + \hat{r}_j) \quad [22]$$

$$\beta_{ds,ij} = \pi(\hat{r}_i + \hat{r}_j)^2 |w_j - w_i| \quad [23]$$

where i, j are indices denoting the two interacting particles and \hat{r}_i, \hat{r}_j are the effective interaction sizes, here defined to be $\lambda_i^{1/D}, \lambda_j^{1/D}$. $\hat{D}_i = kT(6\pi\eta\hat{r}_i)^{-1}$ is the Brownian diffusion coefficient for the i particle, with T the absolute temperature, k the Boltzmann constant, γ the average turbulent shear, η the dynamic viscosity, and w_i, w_j the particle fall velocities (19).

The particle excess mass was used for m . For the monomer, the excess mass is the total particle mass less the mass of water displaced by the particle. The net gravitational force on a particle is proportional to its excess mass.

The settling rate w_i was calculated assuming a balance between gravitational and drag forces:

$$w = \frac{gm}{6\pi\eta\hat{r}_i} \quad [24]$$

where $\hat{r}_i = \lambda_i^{1/D}$.

The system was completed by adding sources of new particles and settling losses of old particles to Eq. [19] in the form of the term

$$I_{kl} - \frac{Q_{k,l}}{Z} \int_{\lambda_{k-1}}^{\lambda_k} \int_{m_{l-1}}^{m_l} n w m \, dm \, d\lambda$$

For the single-source simulations,

$$I_{1,1} = \mu Q_{1,1}$$

$$I_{k,l} = 0 \quad \text{for } (k, l) \neq (1, 1)$$

For the two-source particle simulations,

$$\begin{aligned} I_{k,l} &= \mu Q_{2,1} \quad \text{for } (k, l) = (1, 2), (2, 1), \\ &= 0 \quad \text{otherwise.} \end{aligned} \quad [26]$$

This formulation of particle growth mimics algal growth dynamics (20).

RESULTS

Coagulation of a Single-Source Particle

Calculating the development of particle size distribution using a one-dimensional sectional approach with a source similar to that of Eq. [25] shows the expected increase and decrease in particle concentrations (Fig. 2A). Using only 10 sections and not allowing matter to leave the system by coagulation of particles in the 10th section results in an

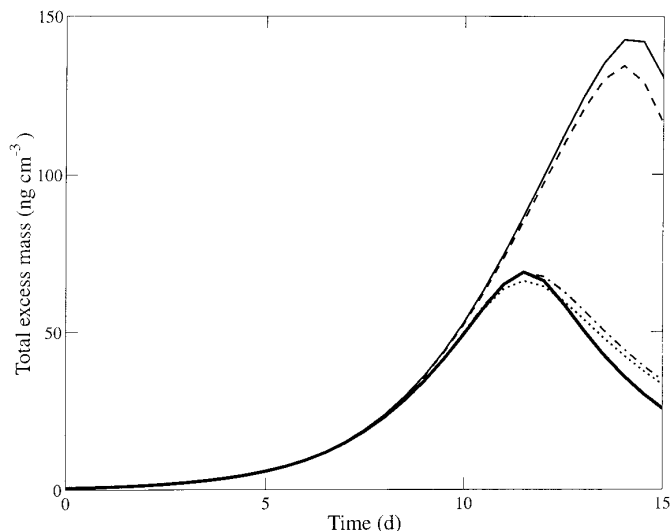


FIG. 3. Total excess mass concentrations in time for different calculation schemes of the two-dimensional spectra. The calculations are as in Fig. 2. — (thick): one-dimensional calculation; — (thin), - - : two-dimensional, diagonally constrained; · · · : two-dimensional, full grid; - - · · · : $\bar{q}_{kl}(t) = Q_{kl}(t)/(\lambda m_{l-1} \ln(2))$; — (thin), - · · : $\bar{q}_{kl}(t) = Q_{kl}(t)/(m_{l-1} \lambda k_{l-1})$.

accumulation of matter in that last section. The abnormally high concentrations in it bias the particle interactions because large particles interact with and remove smaller particles from other sections more rapidly, suppressing the accumulation of matter in smaller particles until the large particles settle out of the system. Simulating a natural situation more realistically would involve adding more sections and including disaggregation of the largest particles.

Casting the system in two dimensions and making the full grid calculation results in a mass distribution that is only slightly different (Fig. 2B) from the one-dimensional simulation. The total mass in the system is almost the same until the material in the last sections begin to dominate, at which point the total mass becomes as much as 25% greater in the two dimensional system (Fig. 3).

Imposing the diagonal constraint on the two-dimensional system results in a larger accumulation of mass through time that is particularly evident when the mass accumulates at the last sections (Fig. 2B, 3). Examination of the interaction terms shows that this results from not allowing collisions between particles from different sections that create new particles that are in off-diagonal sections. As a result of the smaller bounds on allowable interactions, the interaction coefficients are smaller. The decreased interaction rates do not affect interactions between particles from the same section because they form a particle that is also on the diagonal. The dominance of collisions between particles in the same section keeps the diagonal and nondiagonal two-dimensional calculations similar.

The formulation of the source term, which is not constant but is proportional to the particles concentration in the first

section, accentuates the differences between the full grid and diagonally constrained systems once they start to diverge. With a different source function, the systems could be more similar.

There is a significant computational cost associated with using the full two-dimensional spectrum rather than just the diagonal case. This is not only because of the larger number of calculations which must be made but also because the larger full case requires tighter error constraints in the calculation. For example, it took 4.4 s of processor time to calculate the interaction coefficients for the diagonally constrained system and 248 s for the full 10×10 grid system using a DEC 3000/600 workstation. Using a larger grid (20×20) for the full grid system resulted in an even longer computation time, 4769 s.

The results were relatively insensitive to the form used to represent \bar{g}_{kl} as a function of λ within a section (Fig. 3).

Coagulation of a Two Source Particles Using the Two-Dimensional Particle Spectrum

The preceding model was modified by adding a second particle source in a different section. The lower value of its λ was half and its m twice that of the original particle source. The grid was expanded to 11×11 to accommodate the new particle source while maintaining the length of the diagonal

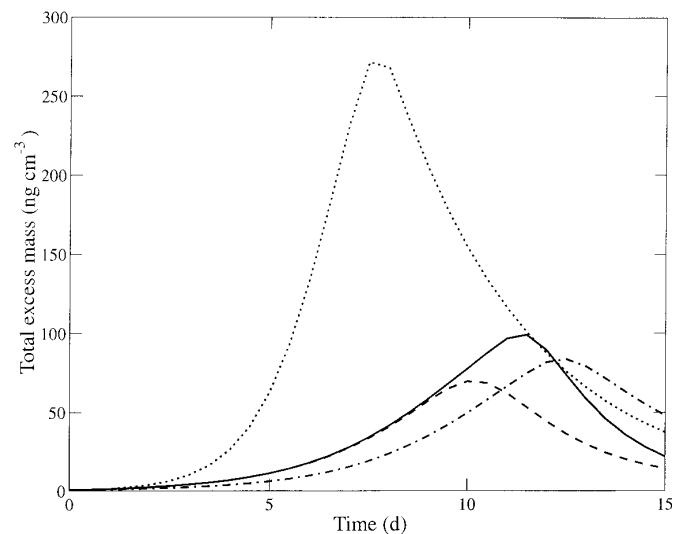


FIG. 4. Total excess particle mass in the presence of two particle sources. The first particle source is the same as that in Fig. 2 and is at $(k, l) = (2, 1)$; the second source has values of m twice as large and λ half as large as those of the first. The source of the first particle is the same as the previous case, $(k, l) = (1, 2)$; the rate of addition of the second particle is the same as that of the first. — : diagonally constrained interactions (see Fig. 1); - - : full grid interactions; - · · : the single source particle, full-grid simulation from Fig. 3; · · · : one-dimensional case $\mu = 1 \text{ d}^{-1}$. The calculation is made for a two-dimensional grid of 11 sections by 11 sections. Because of the size relationships of the two source particles, there are 10 sections along the diagonal for each source particle.

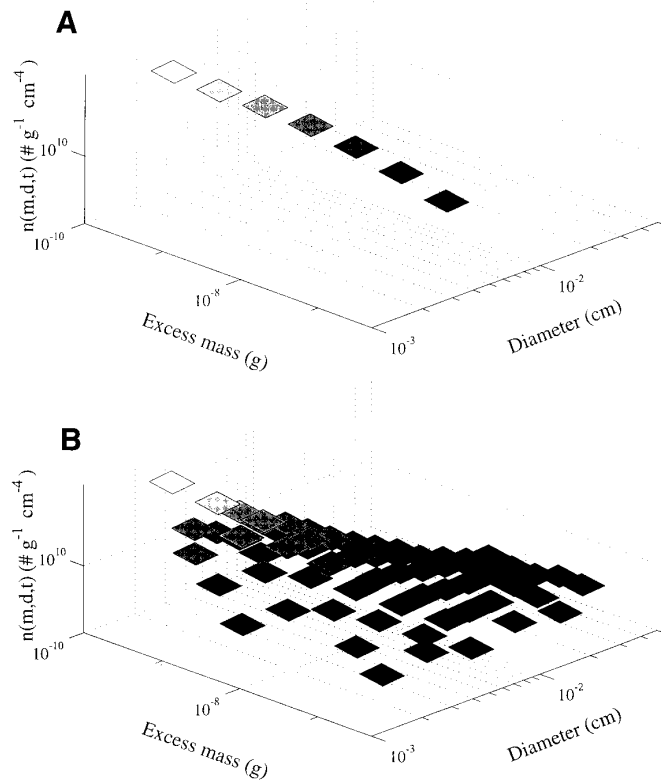


FIG. 5. Two-dimensional particle size spectra for one source particle at $t = 10$ d. The spectra consist of patches which have constant shape within the lower and upper sectional bounds whose shading darkens for smaller values. The particle size spectra as a function of excess mass and particle diameter is calculated from computational results by using $n(m, d, t) = n(m, \lambda, t) \cdot (d\lambda/dd)$. A: diagonal constrained interaction; B: full grid interaction. These represent the cases shown in Fig. 2C, B.

associated with the original particle source at 10 sections. In the new grid, the original source is in section $(k, l) = (2, 1)$, while the new particle source is in section $(k, l) = (1, 2)$. Particles could interact with other particles in the sections along three diagonals in the DC case: diagonals associated with each of the source particles and a diagonal between them (e.g., Fig. 1). The input rate for the new source was the same as for the original particle source (Eq. [26]). Thus, new particle production remained proportional to the concentration of the original particle source, although now twice as fast.

The total excess mass was almost the same in the diagonally constrained and the full grid simulations. The two systems diverged slightly only at $t = 11$ d, when the mass accumulated in the largest section (Fig. 4). One difference between the one and two source particle simulations was the increased mass input rate associated with the model formulation, which is manifested as a more rapid increase in total biomass. However, the maximum particle concentration for the one and two source FG simulations were essentially the

same. An increase in the addition rate for the single-source particle system not only increased the total particle concentration early in the simulation but also increased the maximum particle concentration (Fig. 4). This difference suggests that increasing the range of particle processes will have a substantial difference on the system dynamics.

Summing the masses for sections with the same m interval reiterates the similarity between the diagonally constrained and full-sectional simulations, particularly before day 11. This similarity is closer than that for the single-source particle simulations (e.g., Fig. 5). Much of this similarity exists because most of the particles do occur along the sections which are allowed in the diagonally constrained sections (Fig. 6).

DISCUSSION

The two most important properties of coagulating particles are their masses and lengths. Extending coagulation theory to describe the dynamics of particles under the heterogeneous conditions of natural waters requires the ability to predict the length of a formed after the collision of two dissimilar

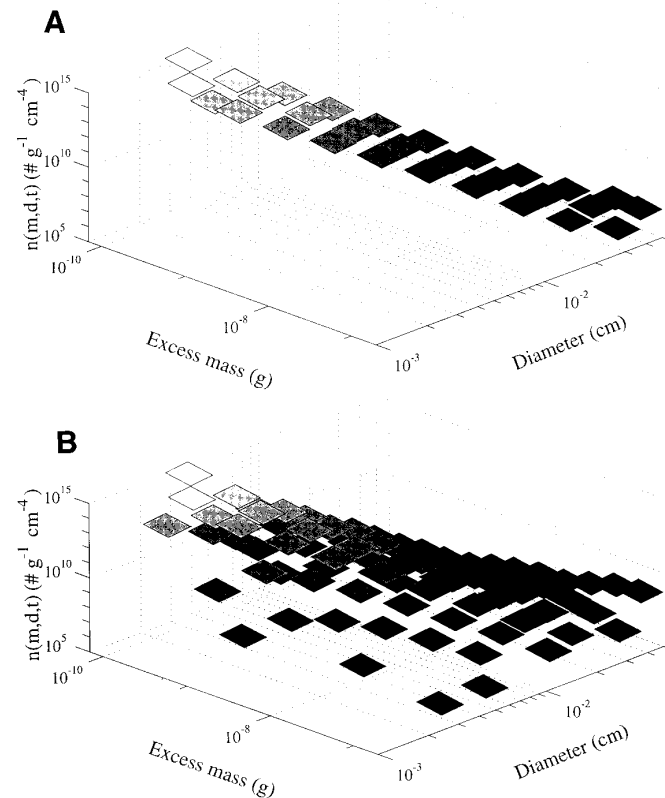


FIG. 6. Two-dimensional particle size spectra for two particle sources at $t = 10$ d. $n(m, d, t)$ calculated as in Fig. 5A: diagonal constrained interaction, in which the allowable region is along three diagonals; B: full grid interaction. The display is for the calculation in Fig. 4.

particles. The new variable put forward here, λ , has the advantages of being conserved in the process of forming a new particle, being simply related to particle length, and being consistent with fractal scaling.

The computational overhead associated with using two-dimensional particle size spectra increases from being proportional to the number of mass intervals approximated to the 2nd power to being proportional to the number of mass intervals to the 4th power. The results presented here suggest that a system can be considerably simplified by considering only the most important interactions without significantly changing the system dynamics.

The ability to represent multiple particle types will be particularly useful in marine systems, where the role of coagulation of regulating phytoplankton populations is an active research area. Experimental observations suggest that production and release of low-density polymeric particles (TEP) is associated with considerably enhanced rates of algal aggregation (e.g., 12, 11, 21, 22). Comparison of rates predicted using aggregation theory requires the ability to describe the interactions between particles with such different sizes and masses as those algal cells and TEP have.

The simple example of two interacting particle sources with slightly different properties presented here suggests that such disparate particles may have different dynamics than those originating from only one particle type. For example, different diameters can increase the collision frequencies for two particles with same masses by giving them different settling velocities and, hence, nonzero differential sedimentation kernels. The resulting increase in coagulation rates creates larger particles at lower source particle concentration, resulting in an increased rate of removal by sedimentation relative to the monodisperse situation. The result of this is a lower total particle concentration for a given particle input rate. Such a change would limit the utility of simple relationships between total parti-

cle concentration and particle removal rate, such as that developed by Farley and Morel (23).

ACKNOWLEDGMENTS

A. Burd provided helpful discussions. This work was supported by Office of Naval Research grant N00014 87-K0005.

REFERENCES

1. Meakin, P., *Rev. Geophys.* **29**, 317 (1991).
2. Vicsek, T., "Fractal Growth Phenomena," 2nd ed. World Scientific, Singapore, 1992.
3. Logan, B. E., and Wilkinson, D. B., *Limnol. Oceanogr.* **35**, 130 (1990).
4. Wietz, D. A., and Oliveria, M., *Phys. Rev. Lett.* **52**, 1433 (1984).
5. Jackson, G. A., *Deep-Sea Res.* **37**, 1197 (1990).
6. Jackson, G. A., *Deep-Sea Res. II* **42**, 159 (1995).
7. Hill, P. S., *J. Geophys. Res.* **97**, 2295 (1992).
8. Alldredge, A. L., and Silver, M. W., *Prog. Oceanogr.* **20**, 41 (1988).
9. Alldredge, A. L., Passow, U., and Logan, B. E., *Deep-Sea Res.* **40**, 1131 (1993).
10. Wells, M. L., and Goldberg, E. D., *Nature* **353**, 342 (1991).
11. Kiørboe, T. P., and Hansen, J. L. S., *J. Plankt. Res.* **15**, 993 (1993).
12. Passow, U., Logan, B. E., and Alldredge, A. L., *Deep-Sea Res.* **41**, 335 (1994).
13. Riebesell, U., *Limnol. Oceanogr.* **37**, 63 (1992).
14. Feder, J., "Fractals." Plenum Press, New York, 1988.
15. Friedlander, S. K., "Smoke, Dust, and Haze: Fundamentals of Aerosol Behavior." Wiley, New York, 1977.
16. Gelbard, F., Tambour, Y., and Seinfeld, J. H., *J. Colloid Interface Sci.* **76**, 541 (1980).
17. Jackson, G. A., and Lochmann, S., *Limnol. Oceanogr.* **37**, 77 (1992).
18. Jackson, G. A., and Lochmann, S. E., in "Environmental Particles," (J. Buffle and H. P. van Leeuwen, Eds.), Vol. 2, p. 387. Lewis Publishers, Boca Raton, 1993.
19. Pruppacher, H. R., and Klett, J. D., "Microphysics of Clouds and Precipitation." D. Riedel, Boston, 1980.
20. Jackson, G. A., *Limnol. Oceanogr.* **34**, 514 (1989).
21. Logan, B. E., Passow, U., Alldredge, A. L., Grossart, H.-P., and Simon, M., *Deep-Sea Res. II* **42**, 203 (1995).
22. Jackson, G. A., *Deep-Sea Res. II* **42**, 215 (1995).
23. Farley, K. J., and Morel, F. M., *Environ. Sci. Technol.* **20**, 187 (1986).